Princeton Plasma Physics Laboratory

PPPL-5354

What Happens to Full-F Gyrokinetic Transport and Turbulence in a Toroidal Wedge Simulation?

C-S. Chang, S. Ku

February 2017

Prepared for the U.S. Department of Energy under Contract DE-AC02-09CH11466.

Princeton Plasma Physics Laboratory
Report Disclaimers

Full Legal Disclaimer

Trademark Disclaimer

PPPL Report Availability

Princeton Plasma Physics Laboratory:

http://www.pppl.gov/techreports.cfm

Office of Scientific and Technical Information (OSTI):

http://www.osti.gov/scitech/

Related Links:

U.S. Department of Energy

U.S. Department of Energy Office of Science

U.S. Department of Energy Office of Fusion Energy Sciences

What happens to full-f gyrokinetic transport and turbulence in a toroidal wedge simulation?

Kyuho Kim,[1] C. S. Chang,[1,2,a)] Jaeghoon Seo,[1,b)] S. Ku,[2] and W. Choe[1]
[1]Department of Physics, Korea Advanced Institute of Science and Technology (KAIST), Daejeon 34141, South Korea
[2]Princeton Plasma Physics Laboratory, Princeton, New Jersey 08543, USA

(Received 18 October 2016; accepted 6 January 2017; published online 24 January 2017)

In order to save the computing time or to fit the simulation size into a limited computing hardware in a gyrokinetic turbulence simulation of a tokamak plasma, a toroidal wedge simulation may be utilized in which only a partial toroidal section is modeled with a periodic boundary condition in the toroidal direction. The most severe restriction in the wedge simulation is expected to be in the longest wavelength turbulence, i.e., ion temperature gradient (ITG) driven turbulence. The global full-f gyrokinetic code XGC1 is used to compare the transport and turbulence properties from a toroidal wedge simulation against the full torus simulation in an ITG unstable plasma in a model toroidal geometry. It is found that (1) the convergence study in the wedge number needs to be conducted all the way down to the full torus in order to avoid a false convergence, (2) a reasonably accurate simulation can be performed if the correct wedge number N can be identified, (3) the validity of a wedge simulation may be checked by performing a wave-number spectral analysis of the turbulence amplitude $|d\mathrm{U}|$ and assuring that the variation of dU between the discrete $k_\parallel$ values is less than 25% compared to the peak $|d\mathrm{U}|$, and (4) a frequency spectrum may not be used for the validity check of a wedge simulation. Published by AIP Publishing.
[http://dx.doi.org/10.1063/1.4974777]

I. INTRODUCTION

In order to save the computing time or to fit the simulation size into a limited computing hardware in a gyrokinetic turbulence simulation of a tokamak plasma, a toroidal wedge simulation is often utilized in which only a partial toroidal section is modeled with a periodic boundary condition in the toroidal direction. In the past, most of the wedge simulations have been performed under simplified delta-f algorithms (e.g., Refs. 1–4 and many others), in which the turbulence is driven by fixed background fluid plasma gradient and in which the neoclassical plasma dynamics is ignored. Recently, global full-f simulations are also beginning to utilize the wedge simulations,[5–8] including XGC1[9,10] that is the code used for this study. A deeper understanding of how the wedge simulations could be similar to or different from the full torus simulations can be beneficial for proper application of the wedge simulations.

A full-f code can perform a different comparison, from what a delta-f code can, between the wedge simulations and the full-torus simulations since it can obtain not only the turbulence properties and the transport fluxes, but also such information in a self-organized state between the plasma profile and the turbulence. Predicting the self-organized plasma profile is the ultimate goal of the plasma transport and turbulence study.

The most severe restriction to the wedge simulation is expected to arise in the longest wavelength turbulence, i.e., the ion temperature gradient (ITG) driven turbulence. In the present work, we study the ITG turbulence and neoclassical ion physics together in the full-f gyrokinetic turbulence code XGC1 in an approximate steady state. Gyrokinetic ions with adiabatic electron response are used in a circular cross-section torus that resembles the so-called Cyclone base-case plasma.[11] Behavior of the ion heat flux, and the resulting self-organized ion temperature profile, with a different toroidal wedge size is reported. Detailed behavior of the turbulence spectrum is also described. As a result of the present study, a simple guideline, to check if a wedge simulation can reproduce the full-torus result within a few percent error, is suggested.

The paper is organized as follows: Section II provides a brief summary of XGC1. Section III describes the simulation setup and the achievement of the approximate steady state. Dependence of the radial heat flux, in the form of effective heat conductivity, and the turbulence spectrum on the wedge size is reported in Secs. IV and V, respectively. Section VI is devoted to conclusion and discussion.

II. A BRIEF SUMMARY OF THE FULL-F GYROKINETIC PARTICLE-IN-CELL CODE XGC1

XGC1 is a "full-f" (or called "total-f," equivalently) gyrokinetic particle-in-cell code[9,10,13] that does not use the perturbative "delta-f" assumption that the background plasma can be described by time-invariant fluid plasma based on the Maxwellian distribution function. In the perturbative delta-f scheme, only the turbulent perturbed part of the distribution function is calculated using moderate number of marker particles ($\sim$50 particles per grid node,

a)Electronic mail: eschang@pppl.gov
b)Present address: Korea Institute of Nuclear Nonproliferation and Control, Daejeon 34054, South Korea

usually). In the full-f kinetic code XGC1, on the other hand, the whole plasma kinetics including the background, neoclassical, and turbulence dynamics are simulated together using large number of marker particles (several thousands of particles per grid node).

XGC1 possesses other special strengths of including the realistic diverted magnetic-field region in the simulation domain, handling the plasma particle loss to the material wall, recycling the neutral particles, and calculating the Monte-Carlo neutral particle transport with a charge exchange and ionization interaction with the plasma. As an ion hit the material wall boundary, it is converted into a neutral atom at Frank-Condon energy (3 eV is used in the present study) with a random initial angle toward the plasma. Since we do not start the neutral particle recycling from their molecular form, we normally prescribe some distance for the birth of the neutral atoms from the divertor plates. XGC1 also includes magnetic axis in the central core. Thus, the simulation domain of XGC1 is the whole volume from magnetic axis to material wall, and across the magnetic separatrix. In a circular model geometry with the outer simulation boundary placed inside the last closed magnetic surface, XGC1 has an option to return the escaping ions back into the plasma by calculating the return point using the conservation of energy and canonical angular momentum. This is the option we take in the present study. The outermost grid nodes are set to a time-constant electrostatic potential (usually zero). When the outermost grid points are on material surface, the Debye potential drop is calculated using a logical sheath method[12] (i.e., an electrically insulated wall condition).

In order to simulate the particle-field dynamics in the complicated edge geometry, XGC1 uses unstructured triangular mesh on each poloidal plane, with the mesh nodes being closely parallel to the magnetic field lines. Generation of field-aligned mesh in a cylindrical coordinate system requires a special and creative scheme. N_{plane}-number of poloidal planes are located at the toroidal angle interval $2p/N_{plane}$. Field-aligned mesh on a flux surface is generated by (1) starting an initial mesh node at a poloidal angle (say, $h = 0$ at outer midplane) on a poloidal plane, (2) copying the initial mesh node at all poloidal planes at the same poloidal angle, axisymmetrically, (3) following the magnetic field line from the initial mesh node to the next poloidal plane in the positive (or negative) poloidal direction to find the next mesh point, (4) copying axisymmetrically this second mesh node at all poloidal planes at the new poloidal angle, and (5) repeating this process until the mesh nodes cover the entire poloidal angle. The last mesh node, in general, will not come back to the initial mesh node exactly. Thus, some minor adjustments can be made in the poloidal angle intervals of the mesh nodes so that the final mesh node coincides with the initial mesh node. The (approximately) field-aligned mesh is then axisymmetric, being identical at all the poloidal planes. In this scheme, the poloidal mesh node interval on a flux surface will be inhomogeneous due to the variation of $B_h=B_/$. The value $B_h=B_/$, thus the mesh node distance, can even approach zero near the magnetic X-point. In this region, is extremely small in this region, this coarsening still yields approximately the field-aligned mesh. When the radial mesh distance becomes too coarse due to a large flux expansion, such as in the vicinity of the magnetic X-point, then we can refine the radial mesh in that subspace, forming a locally field-aligned mesh structure.

The magnetic and wall geometry can be read into XGC1 from a realistic experimental analysis data in the form of the equilibrium fitting (EFIT) g-eqesk file,[14] or from an analytic description. For more detailed information of the full-f XGC1 code that is most relevant to the present work, we refer the readers to Ku et al.[9,10]

The full-f XGC1 gyrokinetic particle code has various simulation options. All of them use gyrokinetic ions. Electrons can be drift-kinetic, gyrokinetic, or fluid. Coulomb collision operation has the fully nonlinear Fokker-Planck-Landau option[15,16] for modeling the non-Maxwellian edge plasmas or the linearized Monte Carlo collision option[9,10,17] for near-Maxwellian core plasmas. The nonlinear Fokker-Planck-Landau collision operator is more expensive than the linearized Monte-Carlo collision operator in the computational cost. In the present study of the ion-temperature-gradient (ITG) driven turbulence, deuteron ions species with adiabatic electron model are used in a circular flux-surface geometry torus. The linear Monte Carlo collision operator is utilized since the pedestal and the scrape-off plasma is not included in the simulation. A core heating and edge cooling is used for heat-flux driven plasma simulation to achieve a (approximate) steady state plasma profile. Particle and momentum sources are turned off for a simpler study of the subject. For the wedge number N (with the whole torus represented by $N = 1$), the total number of marker particles are reduced by 1/N. Sources and sinks are also reduced by 1/N. Five simulations at different N ($N = 1, 2, 3, 6, 12$) are compared using an identical initial plasma profile and magnetic equilibrium.

III. SIMULATION SET UP AND THE APPROXIMATE STEADY STATE

Since XGC1 is a full-f code, the plasma profile (ion temperature profile in this case) evolves to reach a self-organized state in response to the turbulence and neoclassical dynamics, and to the heating and cooling sources. For the present study, the simulation is set up as follows. We use a toroidal concentric circular magnetic geometry: $B_0 = 1.14$ T at magnetic axis, $R_0 = 1.7$ m; $a = 0.4$ m; $a=R_0 = 0.235$; $q = 0.85 p 2.18 dr=a p^2 = 0.85 p 39.264 dr=R_0 p^2$, where B, R, a, q represent the magnetic field strength, major radius, minor radius, and safety factor, respectively. The subscript "0" denotes the magnetic axis position. These parameters are chosen to yield a similar q and its shear to the conventional Cyclone geometry.[11] However, a smaller a/R_0 value is used to reduce the computing time (the plasma minor radius a is reduced from 0.61 m of the Cyclone case to 0.40 m for $R_0 = 1.7$ m chosen here, or a/R_0 is reduced from 0.36 to 0.235). Deuterons are used for the ion species. At the deuteron ion temperature $T_D = T = 1$ keV, we have $q^* = q_i/$

B ¼ B_0. The whole toroidal domain is decomposed into 96 poloidal planes. Thus, a wedge simulation has 96/N poloidal planes covering $0 ::: \phi < 2p=N$, where ϕ is the toroidal angle and N ¼ 2, 3, 6, and 12 for the N 6¼ 1 cases. On each poloidal plane, the mesh distance is 4 mm in the radial direction and 3 mm in the poloidal direction, resulting in 55,763 mesh nodes on each poloidal plane. About 1,500 deuteron marker particles are initiated per mesh node, on the average. Convergence studies show that this many particles are needed to yield enough statistics for full-f particle simulation of ITG turbulence in this larger aspect-ratio circular geometry. In realistic separatrix geometries with kinetic electrons, we often use more number of particles per mesh-node per species. Total number of ion marker particles for the full-torus simulation (N ¼ 1) is about $8x10^9$, with a reduction to $8x10^9$/N for the wedge simulations. Radial domain is set as $0 ::: W_N ::: 0.9$, where W_N is the normalized poloidal flux with zero r ¼ 0 and unity at r ¼ a. We supply 3 MW of ion heating in the core region, $0 ::: W_N ::: 0.35$, and 3 MW cooling in edge region, $0.8 ::: W_N ::: 0.9$ for the full-torus simulation (N ¼ 1). For wedge simulations, the heating and cooling power are reduced to 3 MW/N. Initial density and temperature profiles are shown in Fig. 1. Electron temperature profile is fixed to the initial ion temperature profile. We initially set R_0/L_n ¼ 2.2 and R_0/L_T ¼ 7.5 over the whole volume in order to induce the growth of ITG modes. The radial gradients around the magnetic axis collapse well before the approximate-equilibrium is reached.

Figure 2 shows the time evolution of radially-averaged plasma heat flux for the full torus case. Each circle is averaged over $0.45 ::: W_N ::: 0.7$ spatially, and Dt ¼ 75**1**s temporally in order to smooth out the shorter-time avalanche fluctuations. The heat-flux saturates to 3 MW, with a bursty behavior (or fast-time averaged avalanche behavior), that is equal to the central heating power, and the turbulence property and T profile reach the approximate-equilibrium without a noticeable change. The avalanche and bursty behavior of heat flux has previously been reported in other full-f simulations.[5,7,10] All the wedge simulations are also performed till the approximate-equilibrium is reached. As an example, the heat flux for N ¼ 6 is depicted in Fig. 3, again showing

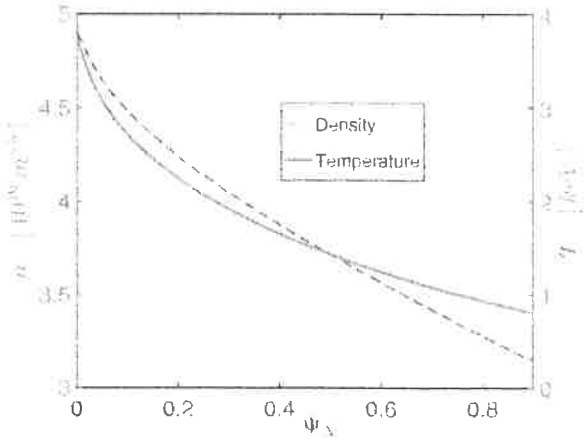

FIG. 1. Initial density n (blue dotted line) and temperature T (red solid line)

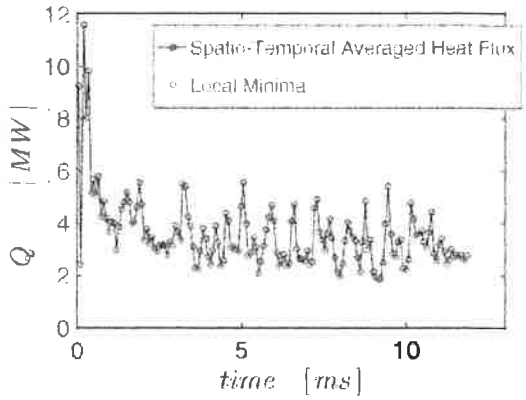

FIG. 2. Radial heat flux versus time for N ¼ 1.

saturation at 3 MW. Compared to the full torus case, the level of bursts is higher and the periods between bursts are longer for N ¼ 6. This appears to be from insufficient nonlinear interactions among different wave numbers in a wedge simulation, as explained later. If we regard the time between two adjacent local minima, marked as red circles, as one burst period in Figs. 2 and 3, the time averaged heat flux over 5 and 10 burst periods in Fig. 4 shows the relative deviation of the heat flux to the input power towards the end of the simulation. It can be seen that the relative deviation from the 10-avalanche averaging is only *rv***6**3% toward the end of the simulation, giving the meaning to our definition of "approximate-equilibrium." All the simulations presented here are performed until this *rv***6**3% imbalance between the heat input and heat out-flow is reached with 10 burst averaging. Likewise, all the physics analyses presented from this point on uses the 10 burst averaging as defined above, unless otherwise stated.

Figure 5 shows the radial profile of the ion temperature T, the ion heat flux Q, the temperature scale length $R_0=L_T$ ¼ $\partial R_0=T\partial dT=dr$, and the effective heat diffusivity v for N ¼ 1 at two different times after reaching an approximate-steady state. Here, r is the plasma minor radius along the outboard midplane and the effective heat diffusivity is defined as $v ¼ -Q=\partial n\, dT=dr\partial$. Between two different approximate-steady times, the difference is ::S3% compared to the maximum value. Figure 5 serves as an uncertainty estimate in the approximate-equilibrium macroscopic quantities obtained

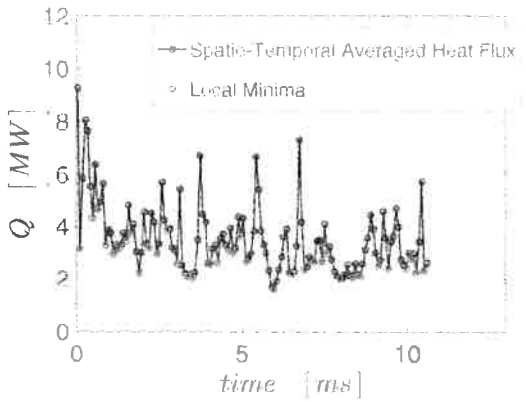

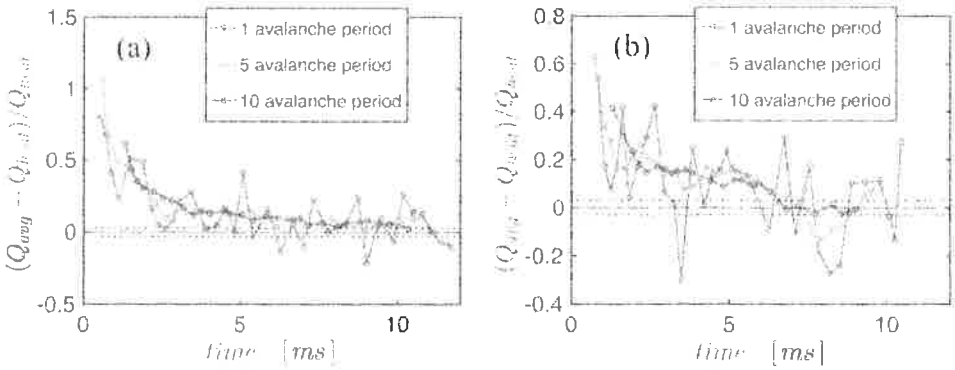

FIG. 4. The difference between heat flux averaged over several burst periods and heat power for (a) N ¼ 1 and (b) N ¼ 6. Black line and black dotted line represent 0 and 6 0.03, respectively.

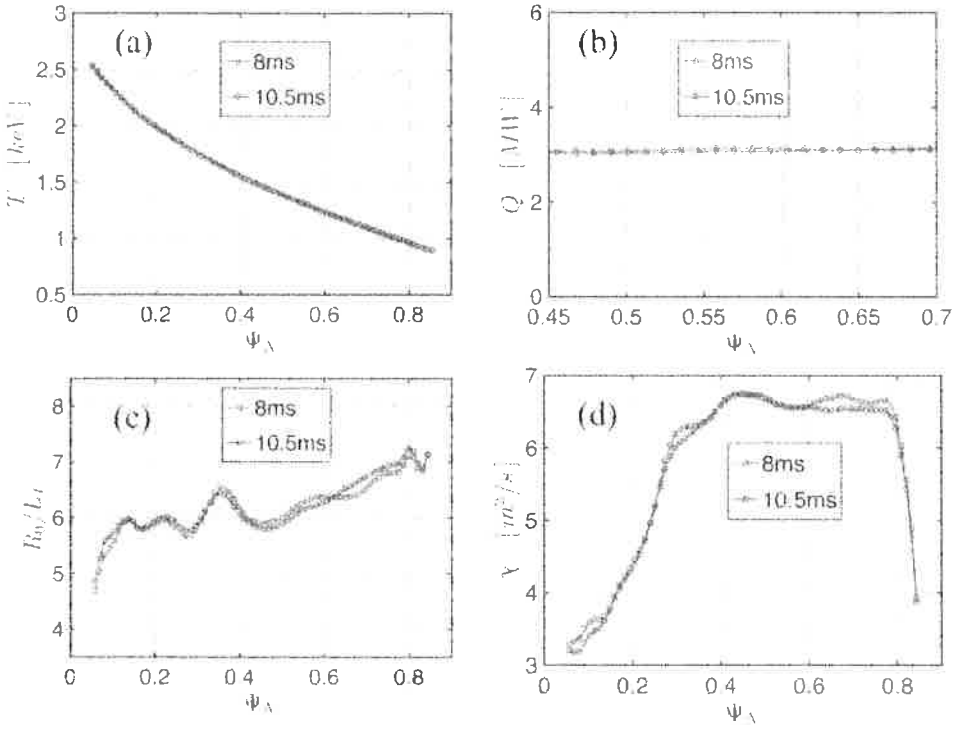

FIG. 5. Comparisons of (a) Temperature, (b) Heat flux, (c) Temperature scale length, and (d) effective heat diffusivity at two different approximate-steady states for N ¼ 1. Red and blue lines are corresponding to approximate-steady states near 8 ms and 10.5 ms, respectively.

from the simulation: For the temperature and heat flux profiles, there is little uncertainty (≪3%). For the temperature gradient and the effective heat conductivity, which are first-order derivative quantitatives, the uncertainty is up to *r*v3%.

IV. COMPARISON OF THE HEAT TRANSPORT BETWEEN THE FULL AND WEDGE SIMULATIONS

In this section, various macroscopic physical quantities—heat flux, temperature, temperature gradient scale-length, and effective heat diffusivity—are compared between the full-torus simulation and the wedge simulations. Heat flux in approximate-steady state in the source-sink free region $0.45 < W_N < 0.70$ are shown in Fig. 6, showing the achievement of an approximate steady state under 3 MW of central heating and 3 MW of edge cooling. Red, green blue, cyan, and magenta lines correspond to full-torus, half-torus, 1/3 torus, 1/6 torus, and 1/12 torus, respectively. Deviations from the heat input power are within or around 63%, showing an achievement of the approximate-steady state to the

In Fig. 7(a), Deuteron temperature T at approximate-steady state is displayed for N ¼ 1, 2, 3, 6, and 12. Because of the edge cooling, the edge temperature becomes similar regardless of the N-values. Temperature profiles for N ¼ 1 and N ¼ 2 are visually indistinguishable over all radial

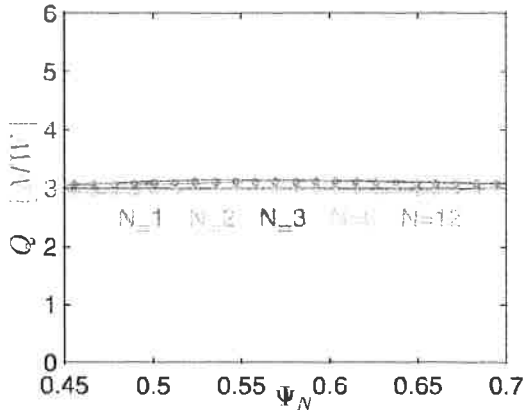

FIG. 6. Heat flux in the source free region for N ¼ 1, 2, 3, 6, and 12 at

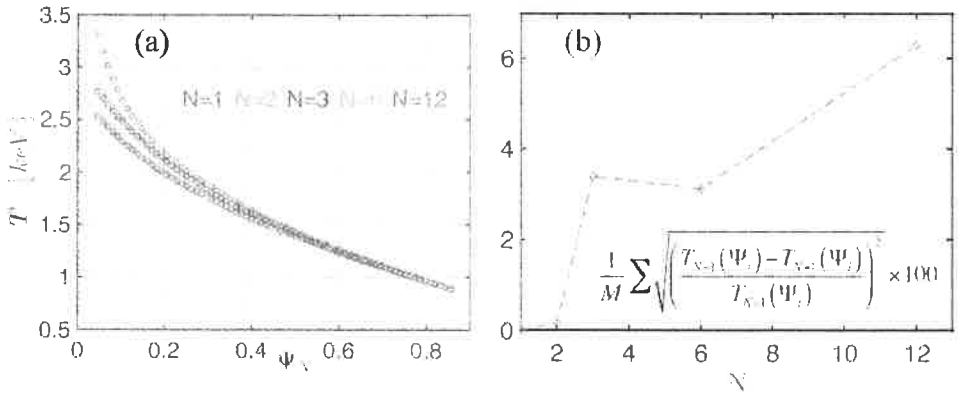

FIG. 7. (a) Temperature at approximate-steady state, and (b) an averaged ratio of temperature difference with full-torus to full-torus temperature.

domains. Temperature profiles for N ¼ 3 and 6 are also almost indistinguishable. Thus, if we consider only N ¼ 12, 6, and 3, it appears that the convergence in the ion temperature profile is achieved at N ¼ 6. However, there is a non-negligible jump between N ¼ 2 and N ¼ 3: about 10% difference in the central temperature. Therefore, the half-torus simulation only can reproduce the full-torus result in this plasma. In order to quantify the convergence, we plot the relative root-mean-square deviation (in the % unit) between N-wedge temperature profile and the full-torus temperature profile in Fig. 7(b): $\frac{1}{M}\sum\sqrt{\left(\frac{T_{N=1}(W_i)-T_{N=n}(W_i)}{T_{N=1}(W_i)}\right)^2}\times 100$, here, M (¼ 72) is the total number of radial points on which the temperature is recorded during the simulation. A false convergence between N ¼ 6 and 3, and the true convergence between N ¼ 2 and N ¼ 1 can be clearly seen.

The important quantity in the self-organization of the ITG turbulence with the background profile is the ion temperature gradient scale length $1=L_T ¼ \partial dT=dr\rho=T$. The dimensionless temperature scale length R_0/L_T is plotted in Fig. 8(a) as a function of minor radius for each N. It can be seen again that R_0/L_T is virtually indistinguishable between N ¼ 1 and 2, except near the magnetic axis W_N ::S 0.1 where the ITG mode is stable and only the non-locally spread fluctuations exist. N ¼ 3, 6, and 12 show a non-negligible or significant difference from N ¼ 1 and 2. Since the radially averaged gradient scale-length is meaningful for the global turbulence and transport, the spatially averaged temperature scale length $\overline{R_0=L_T}$ is depicted in Fig. 8(b) for each N for a quantification of the convergence. It can again be seen from Fig. 8(b) that the convergence from N ¼ 6 and 3 is a false one. Only the convergence from N ¼ 2 to 1 is the true one.

Similar conclusion can be made from the effective heat diffusivity v and the spatially averaged v in Fig. 9. All these analyses show that the half-torus simulation is needed in order to obtain a high-fidelity result in the modeled plasma. However, for an approximate study allowing for *rv*10% error in the central temperature, N ¼ 6 can be used.

V. COMPARISON OF TURBULENCE SPECTRA BETWEEN THE FULL AND WEDGE SIMULATIONS

It is of interest to understand how the turbulence solution changes and why the transport becomes different as the wedge size becomes smaller. In Fig. 10(a), the radially averaged k_h spectrum of the turbulent electric potential is displayed, where k_h represents the poloidal wave number. The radial average is performed over 15 radial points, W_N ¼ 0:05; 0:1; 0:15; ...; 0:75. In Fig. 10(b), the area under the turbulence intensity curve du_k^2 is plotted together with the radially-averaged effective heat diffusivity ¥. Both figures confirm that the turbulence solution converges at N ¼ 2, not at N ;:: 3. Convergence of ¥ is similar to the convergence of the turbulence energy du^2, as expected.

A more detailed understanding of the turbulence property can be obtained by analyzing the k_h spectrum at one radial location, especially on a mode rational surface. Figure 11 shows the turbulence spectrum on the q ¼ 1.5 surface, which corresponds to W_N 0.45, and r 0.22 m. The local turbulence intensity becomes spiky in k_h as N increases. As can be seen from Fig. 11, only the toroidal mode number n ¼ 0, N, 2N; ... can be captured in the wedge simulations. The k_h(¼ nq/r) value of the resolved modes in the wedge simulations, thus, can be expressed as multiples of Nq/r. Thus, Dk_h ¼ Nq/r between the local maxima in the k_h

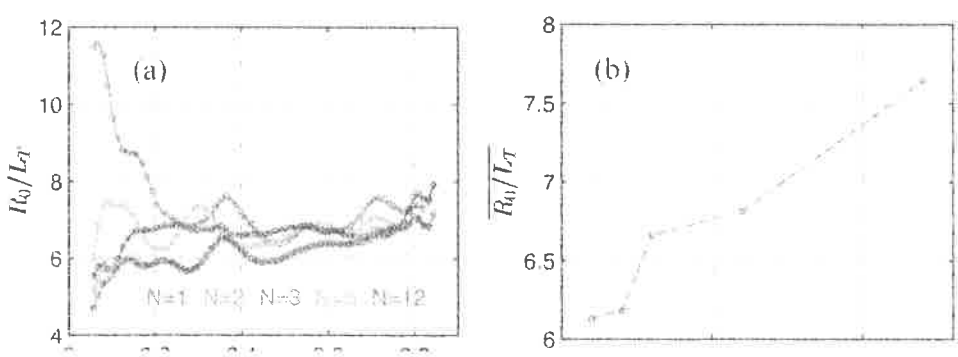

FIG. 8. (a) Temperature scale length, R_0/L_T, and (b) the spatial averaged temperature scale length.

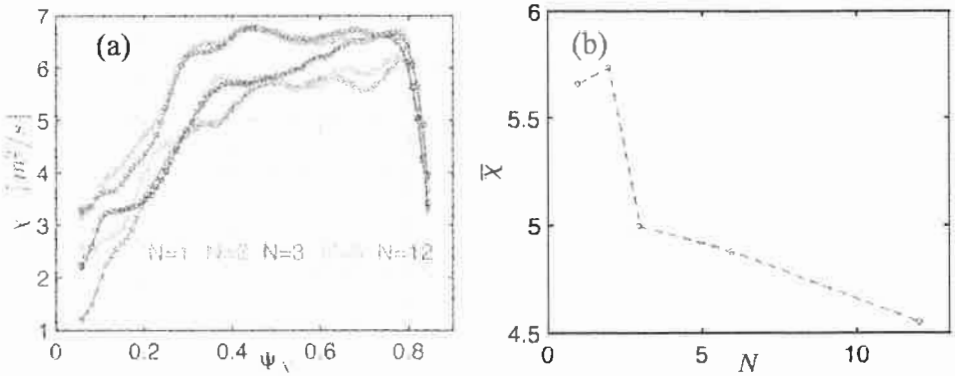

FIG. 9. (a) Effective ion heat diffusivity and (b) spatially averaged heat diffusivity.

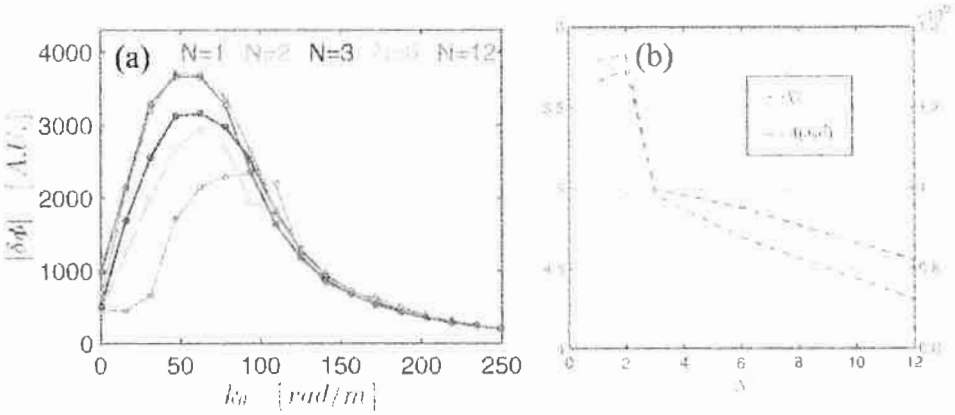

FIG. 10. (a) Spatially averaged k_h spectrum and (b) comparison of spatially-averaged effective heat diffusivity χ and the area under turbulence intensity du_k^2.

spectrum becomes approximately 20, 40, and 80 (rad/m) for N ¼ 3, 6, and 12, respectively. This is described as blue, cyan, and magenta arrows in Fig. 11. It can be seen that the k_h spectrum for N ¼ 2 approximately follows that of N ¼ 1 throughout the entire k_h range, with the fluctuation between different k_h values being less than 25% compared to the maximal turbulent *j*dU*j*. However, the spectrum for N ¼ 3 deviates significantly from that of N ¼ 1 at a lower k_h range where most of the turbulence energy resides, and the heat transport is driven. The fluctuation between different k_h values is noticeably greater than 25%, compared to the maximal turbulent *j*dU*j*.

It is interesting to notice that the frequency spectrum is less sensitive to the wedge number than the wave-number spectrum, as can be seen from Fig. 12(b). N ¼ 1, 2, and 3 show a similar frequency spectrum. Thus, the use of the frequency spectrum to measure the validity of the wedge simulation can yield an erratic conclusion. The reason for this observation can be understood from Fig. 13, plotted at W_X *r*/*v* 0.45. Even though the k_h spectrum shows a discrete behavior, the frequency spectrum shows overlaps. Figure 13 also shows gaps in the k_h spectrum in the wedge simulations. Only N ¼ 2 case shows a relatively insignificant gap between the discrete k_h spectra in the model plasma used here.

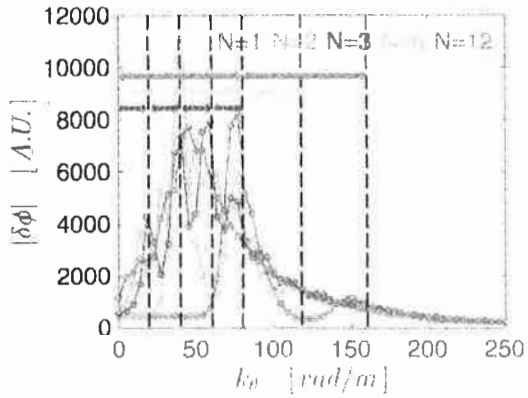

FIG. 11. k_h spectrum of N ¼ 1, 2, 3, 6, 12 at q ¼ 1.5, W_X 0.45, and r 0.22 m surface. Black dotted lines coincide with the local maxima of N ¼ 3, 6, and 12. Blue, cyan, and magenta arrows have a length of 20, 40

Note here that the degree of gap between the discrete k_h spectra is determined by the gap distance Dk_h ¼ Nq/r and the turbulence spread in the k_h direction at each discrete k_h values, which can be a function of plasma equilibrium (e.g., distance between mode rational surfaces, ion gyroradius q_i, magnetic shear, and others). For the same q, the relation Dk_h ¼ Nq/r states that the gap distance becomes smaller at greater r and the turbulence physics states that the spread in k_h is proportional to q_i. Thus, the convergence wedge number N can be greater than 2 in the normal cyclone geometry where the plasma minor radius is 1.5 times greater, and the ion gyro-radius is also greater by the same factor for the common a/q_i ¼ 100 ratio. Thus, N ¼ 2 for the valid wedge size is a rather conservative number for conventional tokamaks with a similar aspect ratio (R_0/a) as the Cyclone base case. The present study suggests, however, a method to identify the validity of a wedge simulation. A wave number spectrum needs to be studied and the fluctuation of *j*dU*j* in the k_h spectrum can be checked to be below 25% of peak *j*dU*j* as a necessary condition for a reliable wedge simulation in a global full-f code such as XGC1. The wedge number N may

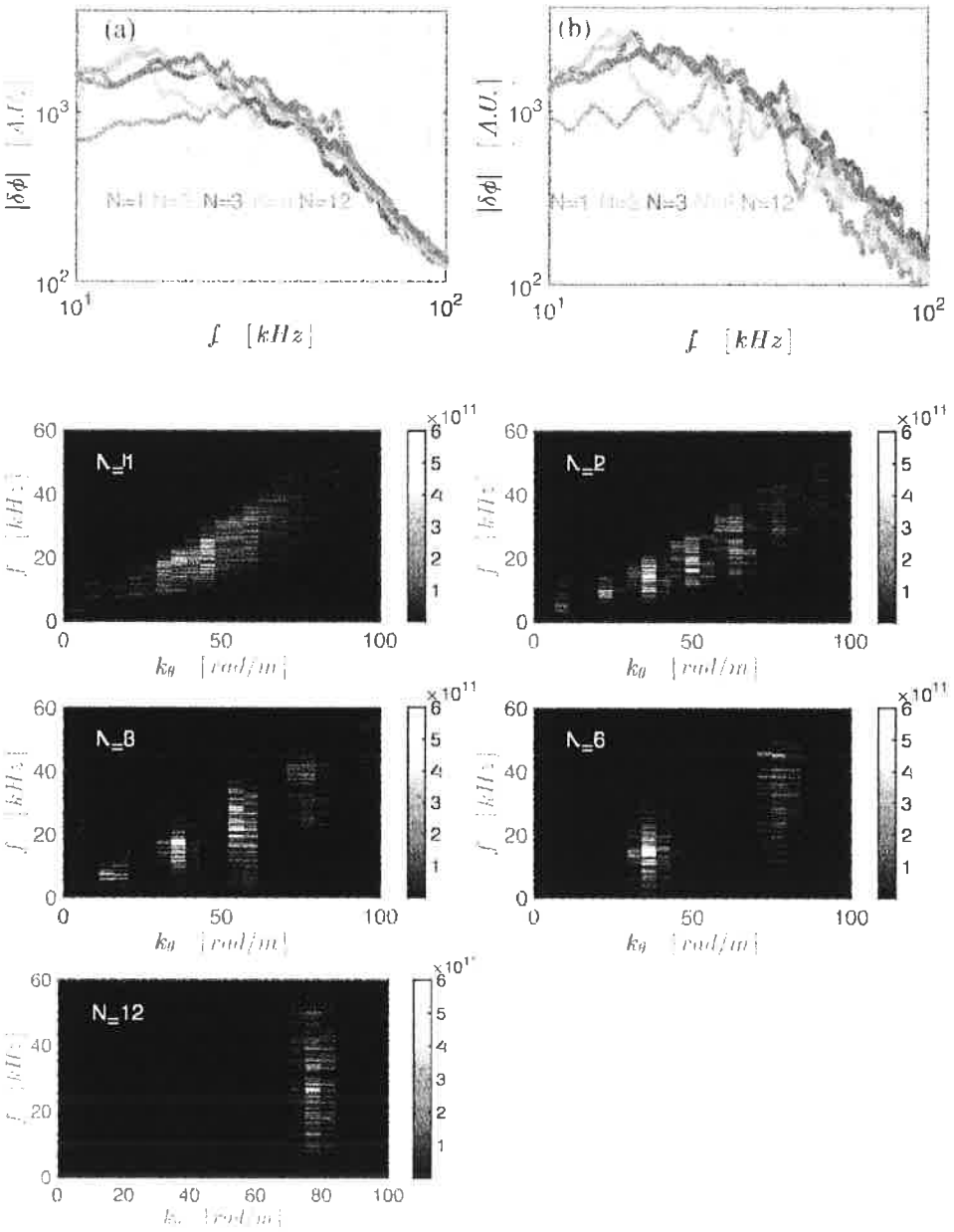

FIG. 12. (a) Spatial averaged frequency spectrum over 15 different radial locations and (b) the frequency spectrum at W_N 0.45 of turbulent potential at outboard mid-plane.

FIG. 13. f – k_h spectrum of turbulent electric potential at $W_N \approx 0.45$.

VI. SUMMARY

Deviation of the thermal transport and the turbulence characteristics caused by a wedge simulation is investigated in the full-f gyrokinetic code XGC1 using a model toroidal geometry. It is found that (1) the convergence study in the wedge number needs to be conducted all the way to the full torus in order to avoid a false convergence, (2) a reasonably accurate simulation can be performed if the correct wedge number N can be identified, (3) the validity of a wedge simulation may be checked by performing a wave-number spectral analysis of the turbulence amplitude $j\mathrm{d}\mathrm{U}j$ and assuring that the variation of $j\mathrm{d}\mathrm{U}j$ between the discrete k_h values is less than 25% compared to the peak $j\mathrm{d}\mathrm{U}j$, and (4) a frequency spectrum may not be used for the validity check of a wedge simulation. However, we also note that this 25% condition in the k_h spectrum has not been thoroughly investigated in various tokamak geometries and can only be used as

ACKNOWLEDGMENTS

This work has been funded by the National Research Foundation of Korea (NRF) under Contract No. NRF-2014M1A7A1A03045191 and by the U.S. Department of Energy under Contract No. DE-AC02-09CH11466. This research used resources of the National Energy Research Scientific Computing Center, a DOE Office of Science User Facility supported under Contract No. DE-AC02-05CH11231. The corresponding author wishes to thank Dr. Y. Idomura for helpful discussions.

[1]W. Wan, S. E. Parker, Y. Chen, R. J. Groebner, Z. Yan, A. Y. Pankin, and S. E. Kruger, Phys. Plasmas 20, 055902 (2013).
[2]R. E. Waltz, J. Candy, and C. C. Petty, Phys. Plasmas 13, 072304 (2006).
[3]B. F. McMillan, X. Lapillonne, S. Brunner, L. Villard, S. Jolliet, A. Bottino, T. Görler, and F. Jenko, Phys. Rev. Lett. 105, 155001 (2010).
[4]L. Villard, P. Angelino, A. Bottino, S. Brunner, S. Jolliet, B. F. McMillan, T. M. Tran, and T. Vernay, Plasma Phys. Controlled Fusion 55, 074017 (2013).
[5]Y. Idomura, H. Urano, N. Aiba, and S. Tokuda, Nucl. Fusion 49, 065029

[6]G. Dif-Pradalier, P. H. Diamond, V. Grandgirard, Y. Sarazin, J. Abiteboul, X. Garbet, Ph. Ghendrih, A. Strugarek, S. Ku, and C. S. Chang, Phys. Rev. E 82, 025401 (2010).
[7]Y. Sarazin, V. Grandgirard, J. Abiteboul, S. Allfrey, X. Garbet, Ph. Ghendrih, G. Latu, A. Strugarek, G. Dif-Pradalier, P. H. Diamond, S. Ku, C. S. Chang, B. F. McMillan, T. M. Tran, L. Villard, S. Jolliet, A. Bottino, and P. Angelino, Nucl. Fusion 51, 103023 (2011).
[8]S. Jolliet and Y. Idomura, Nucl. Fusion 52, 023026 (2012).
[9]C. S. Chang, S. Ku, P. H. Diamond, Z. Lin, S. Parker, T. S. Hahm, and N. Samatova, Phys. Plasmas 16, 056108 (2009).
[10]S. Ku, C. S. Chang, and P. H. Diamond, Nucl. Fusion 49, 115021 (2009).
[11]A. M. Dimits, G. Bateman, M. A. Beer, B. I. Cohen, W. Dorland, G. W. Hammett, C. Kim, J. E. Kinsey, M. Kotschenreuther, A. H. Kritz, L. L. Lao, J. Mandrekas, W. M. Nevins, S. E. Parker, A. J. Redd, D. E. Shumaker, R. Sydora, and J. Weiland, Phys. Plasmas 7, 969–983 (2000).
[12]S. E. Parker, R. J. Procassini, C. K. Birdsall, and B. I. Cohen, J. Comput. Phys. 104, 41 (1993).
[13]S. Ku, R. Hager, C. S. Chang, J. M. Kwon, and S. E. Parker, J. Comput. Phys. 315, 467–475 (2016).
[14]L. L. Lao, H. St. John, R. D. Stambaugh, A. G. Kellman, and W. Pfeiffer, Nucl. Fusion 25, 1611 (1985).
[15]E. S. Yoon and C. S. Chang, Phys. Plasmas 21, 032503 (2014).
[16]R. Hager, E. S. Yoon, S. Ku, E. F. D'Azevedo, P. H. Worley, and C. S. Chang, J. Comput. Phys. 315, 644–660 (2016).
[17]G. Park, C. S. Chang, I. Joseph, and R. A. Moyer, Phys. Plasmas 17, 102503 (2010).

PPPL PRINCETON PLASMA PHYSICS LABORATORY

Princeton Plasma Physics Laboratory
Office of Reports and Publications

Managed by
Princeton University

under contract with the
U.S. Department of Energy
(DE-AC02-09CH11466)

P.O. Box 451, Princeton, NJ 08543
Phone: 609-243-2245
Fax: 609-243-2751

E-mail: publications@pppl.gov

Website: http://www.pppl.gov